Modeling The airflow Properties around Teardrop for Different Tail Lengths

Salem Omran Adeilla
Mechanical Engineering. Higher Institute of Comprehensive Vocations
Gharian, Libya
Salem_279@yahoo.com

Islam Kamel Shahboun
Mechanical Engineering, Aljabal Algharbi University
Gharian, Libya
Kamel20122011@gmail.com

Hesham Baej
Mechanical Engineering, Higher Institute of Comprehensive Vocations
Gharian, Libya

Abstract **This paper provides a CFD comparison of tow turbulence modeling approaches (SST) and (K-epsilon), with application to the simulation of a teardrop. As well as, the study investigates and compares among 3 different models in a range these types in order to assess the suitability of CFD for use when calculating drag co-efficient. Moreover, the study focuses on 3 different velocities to be impacted with the drag co-efficient. Whereas, the pressure over the body was used to calculate the drag co-efficient for each of the 3 teardrops shapes.**
.

Index Terms— **Teardrop, CFD, Turbulence Model, Drag Co-efficient.**

I. INTRODUCTION

Aerodynamics is one of the important influences on a teardrop. Engineers can determine the aerodynamics of a teardrop by studying how airflow will pass over, under and around the teardrop. The teardrop will move fastest, when it disturbs as little air as possible. Specifically, aerodynamicists measure two variables, down force and drag force. Down force is the amount of downward pressure that influence on the top of teardrop at high speeds. Drag is airflow that slows a teardrop down because of friction caused as air flows over various surfaces of the teardrop[1].

Computational Fluid Dynamics (CFD) is a design tool that has been developed over the past few decades and will be continually developed as the understanding of the physical and chemical phenomena improves. The aims of CFD are to be able to accurately predict fluid flow, heat transfer and chemical reactions in complex systems, which involve one or all of these phenomena. CFD is a computer-based technology that studies the dynamics of all things that flow [2].

In teardrop applications, CFD involves a computer-simulated model of teardrop and then applying the laws of physics to the virtual prototype to predict what the down force or drag may be on various components of the teardrop and how it will respond in various wind conditions and changing environmental conditions [3].

Aerodynamicists can use CFD to better visualize and enhance their understanding of how various designs will perform. It also allows them to experiment with more design variables in a shorter amount of time until they reach optimal results[4].

CFD allows engineers to use computer software to divide components of a teardrop into specific cells or grids (Mesh). For each of those cells, supercomputers are then used to calculate mathematical equations that compute the velocity and air pressure of the wind as it rushes over, under and around the specified components of the teardrop[5].

Aerodynamicists can use the resulting data to compute the drag force which depend on different environmental conditions and different design variables. When the calculations are completed, the aerodynamicists can analyze the results either numerically or graphically. The drag force of an object depends on its shape[5].

Researchers and aerodynamicist have found that the teardrop shape round at the front and a pointed tail at the back to be the most efficient in getting through the air. This can be measured from the drag it produces. Aerodynamic efficiency can be assessed by the drag coefficient, defined via Equation 1.

$$C_D = \frac{F_D}{0.5\rho A V^2} \quad (1)$$

To simplify comparison of the cases, the drag is usually presented as the difference in drag counts (*DC*) between the specific case and the reference case. Drag counts is calculated according to Equation 2.

$$DC = \Delta C_d . 1000 \quad (2)$$

Where;

$$\Delta C_d = C_{D\ specific\ case} - \Delta C_{D\ reference}$$

Whereas the drag force is the density of the air, the air approach velocity and the cross sectional area of the teardrop as seen by the air flow.

This article focuses to apply the effectiveness of CFD to calculate the drag co-efficient of a teardrop for different tail lengths. For the teardrop shape it can be expected to see a low drag co-efficient of around 0.03-0.05. It is known that L/D = 4.5 gives the best drag co-efficient.

As well as, in this study 3 different models were applied in a range of flow types in order to assess the suitability of CFD for use when calculating drag co-efficient. Moreover, the study has also used 3 different velocities. Therefore, this should be impacted with the drag co-efficient.

II. Computational Set up

A. Model Geometry

There are 3 teardrop models; each one had a different tail length, as shown in table-1.

Table 1 Geometry Details

	R (mm)	L_{model} (mm)	Cut off tail (mm)
A	25	50	0.5
B	25	200	2
C	25	250	2.5

This geometry was found from first running 2D analysis of the teardrop shape and making sure that none of the contour plots created went outside of the domain. The resulting contour plot was used to assess that the best size of bounding box was 300mm from the centre of the teardrop cap, 700mm behind it, 500mm above, below and to the sides of the teardrop. The sizing of the bounding box was a balance between correctly measuring the flow impacts over a large area and not making the bounding box too large so that the mesh would have to be coarse. In figure-1, it can be seen that there are pressures that go out of the bounding box, whereas the pressure curves go close to the bounding box, that almost become straight lines which affected by the boundary even if it set to symmetry. In addition, the inlet should be bigger since the pressures which take place are not zero. Finally, close to the outlet a correct result would have an almost straight line representing the final line of the pressures where on its right side, the pressure would be zero.

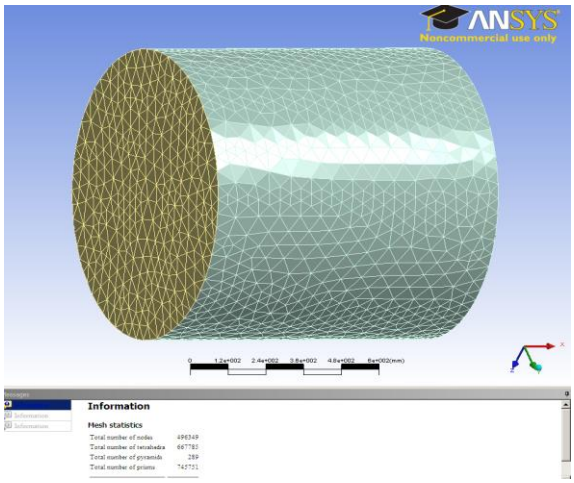

Figure 1 .Trail of circular bounding box.

The model was run at 3 different speeds based on 3 different levels of Reynolds number. The speeds were found by setting the Reynolds number to a specific flow type. The Reynolds number formula was rearranged to calculate the corresponding velocity.

B. Mesh

When creating such mesh it is important that y+ ≈ 1, normalized distance to the wall surface from the centre of the first computational cell. It is also important to ensure sufficient nodes are placed across the boundary layer. It can be demonstrated that in real life a tear drop has a much smaller drag coefficient than a cube. Therefore, it can be presume that, any eddies created by the teardrop should occur near to the surface of the teardrop. For this reason, it is important to model the boundary layer as best possible.

The aim to achieve a y+ value of 5 or lower close to the wall to ensure that it could model the laminar sub layer properly. To mesh this, it can be created a face spacing on the body as well as an inflated layer. It must be taken into consideration that the turbulence model was using is the SST model, the accuracy at modelling the boundary layer. As well as the inflation layer which changed the default face spacing, maximum body spacing and default mesh size, were to enable incorporating such a large mesh size and to limit the number of cells located further away from the body.

The concentration of the nodes in relation to the bounding box can be demonstrated in Figure -2 below. Through these screenshots it is possible to see that the cells near the wall of the body are highly concentrated and the concentration of the cells reduces significantly the further out from the body that the cell is located.

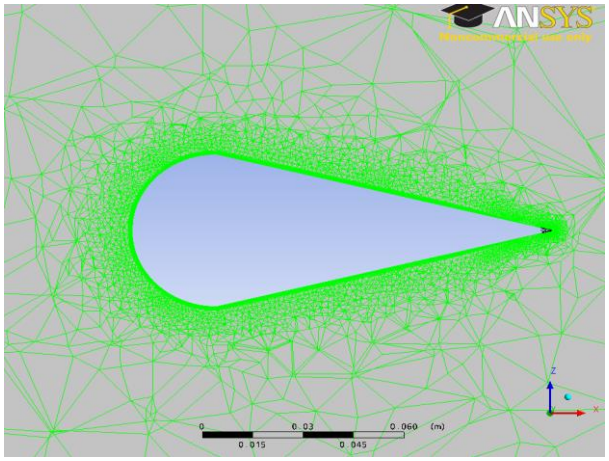

Figure 2. Mesh Density

C. Turbulence Models

For this analysis, SST was used for modeling the boundary layer close to the body. Therefore, SST is the most appropriate turbulence model for use. At low Reynolds number, the SST and k-epsilon turbulence model data were compared to no turbulence model and SST was found to give most similar results to the no turbulence model run. This confirms the use of SST for this analysis. Although a range of transitional models are available in Fluent, these all typically behave in a similar manner, thus Transition SST was chosen as representative. The continuity equation finds the velocities u, v and w. In order to find pressure the 3 equations are discredited and solved together. 3 velocities are applied to the models, in this case, u is specified, v and w are set to 0 m /s.

III. Results

Pressure and fluid velocities are always calculated in conjunction. Pressure can be used to calculate forces on objects. For the prediction of drag of a teardrop. Fluid velocities can be visualized to show flow structures. From the flow field, it can be applied other variables such as shear and vorticity. Shear stresses may relate to erosion of solid surfaces. Deformation of fluid elements is important in mixing processes. Vorticity describes the rotation of fluid elements. In turbulent flows, turbulent kinetic energy and dissipation rate are important for such processes as heat transfer and mass transfer in boundary layers. For non-isothermal flows, the temperature field is important. This may contain evaporation, combustion, and other processes. Results are usually reviewed in one of two ways, graphically or alphanumerically. Graphical analysis options include; vector plots, contours, iso-surfaces, flow lines, animation. Alphanumeric options include; integral values, drag, lift, torque calculations, averages, standard deviations, minimum, maximum, compare with experimental data, In a fluid flow field, each fluid element undergoes three different effects; translation, deformation and rotation. Pressure can be used to calculate forces such as drag, lift and torque on objects by integrating the pressure over the surface of the object.

Pressure consists of three components such as, Hydrostatic pressure ρgh, dynamic pressure ρv2/2 and Static pressure Ps. This can be further divided into an operating pressure such as, atmospheric pressure and a gauge pressure. When static pressure is reported it is usually the gauge pressure only. Total pressure is the static pressure plus the dynamic pressure.

A. Velocity Distribution

Figure-3 below shows the teardrop with 250 mm tail length at velocity of 233.67m/s. The figure indicates, as expected that, the fluid layer at the teardrop boundary is stationary. This is in a bid to assume the stationary position of the teardrop (velocity = 0). Thus, it respects the boundary layer concept.

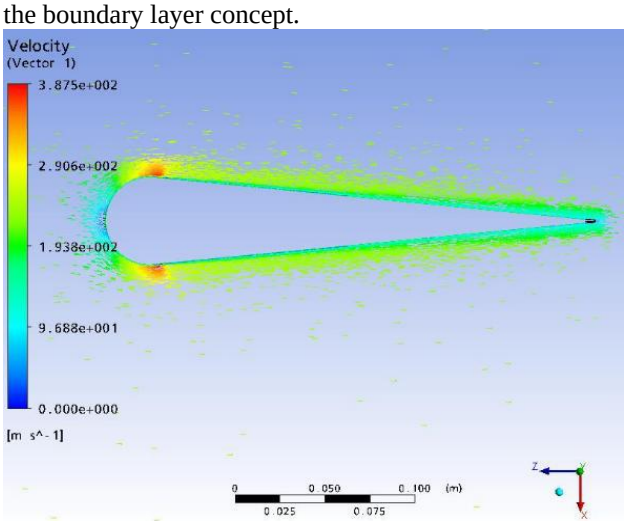

Figure 3 Velocity (233.67 m/s) distribution of 250 mm tail length

Figure-4 indicates that at different spots at the boundary the fluid has velocities ranging from about zero to 100 m/s. This is expected looking at the high velocity of flow round the teardrop. The velocity is high enough to overcome any shear resistance to fluid flow due to the boundary.

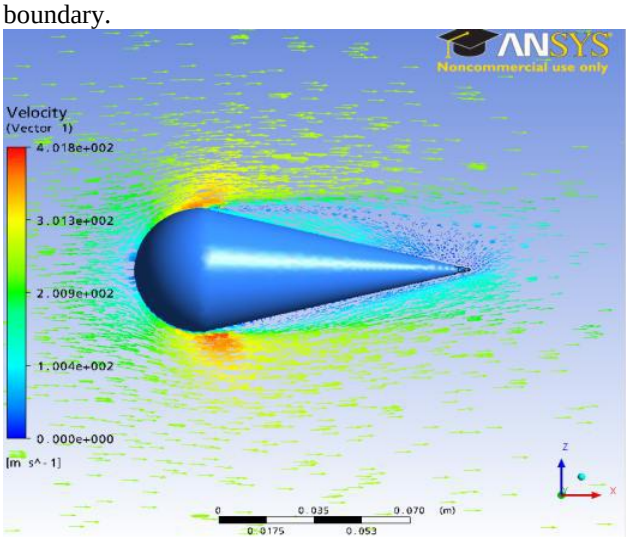

Figure 4. Velocity (233.67 m/s) distribution of 200 mm tail length

However, figure-5 indicates that this layer of the fluid at the boundary (forming the boundary layer) is extremely thin and is almost non-existing at certain locations on the tail.

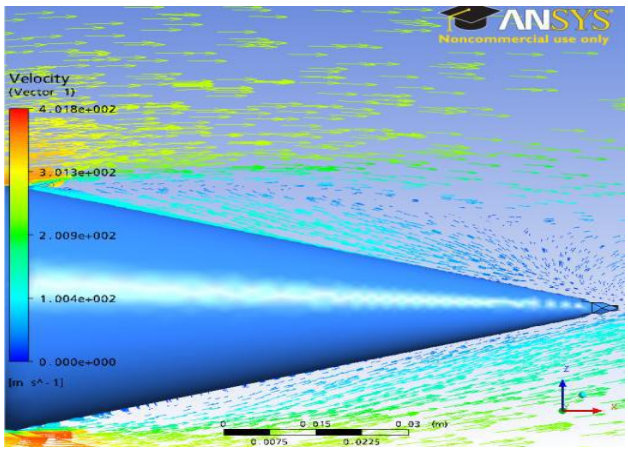

Figure 5. Velocity (233.67 m/s) distribution of 200 mm tail length (close up)

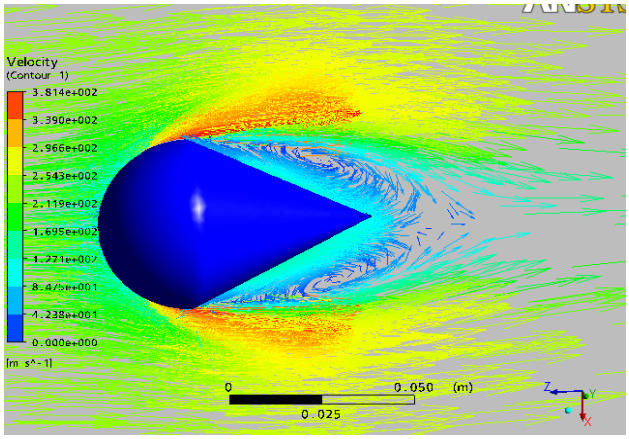

Figure 6. Velocity (233.67 m/s) distribution for 50 mm tail length

As well as, figure-6 demonstrates the airflow decelerating at the shapes leading edge, followed by acceleration around the shapes surface to its maximum velocity (the deepest red colored arrows). The flow can be seen to be recirculation behind the shape, and vortex shedding would be likely to occur in this region.

Intermediate velocity case (v = 116 m/s) also reflect a performance that is intermediate in nature between the performance at the two velocity extremes.

At low velocity of (0.0058 m/s) that applied to the boundary layer is appreciable and the fluid within this layer can be seen to be significantly stationary. Moreover, due to the fact that the velocity at this instance is low, there is a smooth transition of velocity from the boundary outwards until the velocity approaches that of the main fluid flow (that is 0.0058 m/s). The low velocity ensures that there is no turbulence especially at the head of the teardrop (where there is intrusion into the fluid body). This observation fits well into the shear flow/boundary layer concept.

Therefore, comparatively, the fluid approaches the mean fluid velocity smoothly at low velocities than in the case when the mean velocity is high as established by the short tail and long tail cases. However, the identified differences are more pronounced with short tails than with long tail cases. For instance, the boundary layer was obviously non-existing in the case of short tail in high velocity fluid whereas a very thin layer still exists for the corresponding case of long tail. The velocity surge was also more pronounced for short tail case than for long tail. Moreover, the boundary layer was appreciable in the short tail low velocity case than in the long tail low velocity case. Thus, comparatively, length of tail also has effect on velocity performance. Longer tail douses the effects that are more visible with short tails cases.

B. Pressure Distribution

Similarly, the pressure distribution varies depending on tail length and mean velocity (v = 233.67 m/s). At high velocities, there are instabilities and pressure variation is more as compared to low velocities. However, the high velocity long tail situation, pressure is the highest at the midpoint of the teardrop head as shown below in figures (7, 8). Therefore, the molecules of the fluid will make the highest impact at this point on the teardrop. This point is somewhat having a perpendicular surface to the direction of fluid flow. As such, the impact is more direct, resulting in high pressure. The impact reduces as the surface of the head tends gradually towards becoming parallel to the direction of fluid flow. The least pressure is recorded just before the point where the tail and the head of the teardrop meet, obviously because the surface is more or less parallel at this point to flow direction. At the point where the tail and head meet, the pressure becomes negative. This is probably because of the shape of the surface at this point. It is more convex and likely repels fluid molecules away rather than allowing it to impound on the surface.

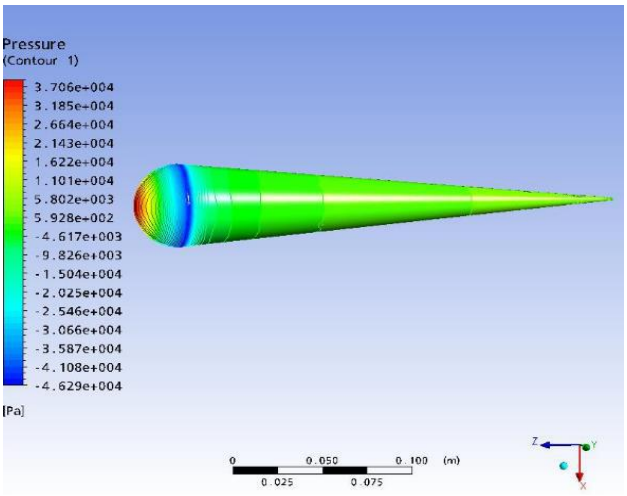

Figure 7.Pressure distribution for 250mm tail length (v=233.67 m/s)

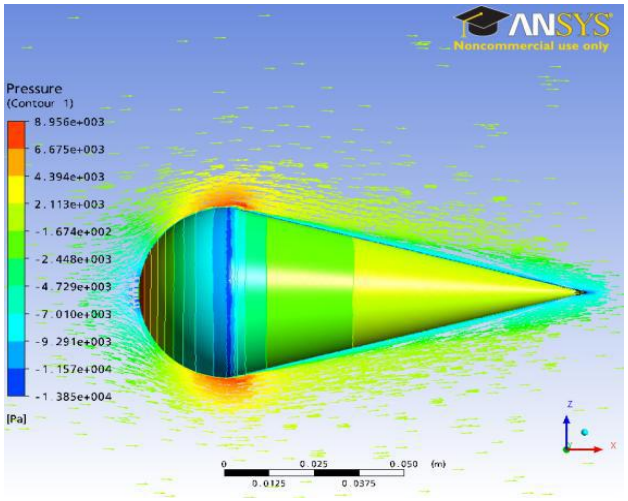

Figure 8. Pressure distribution for 200 mm tail length (v=233 m/s)

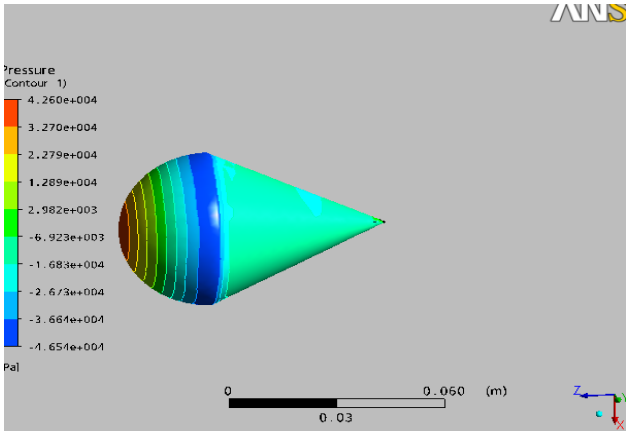

Figure 9. Pressure distributions for 50 mm tail length (v=233 m/s)

This same trend is observed for the high velocity short tail case as shown in (figure-9). However, the shortness of the tail resulted to having a more uniform pressure distribution at the tail than for the long tail situation (compare figures 7, 8 and 9).

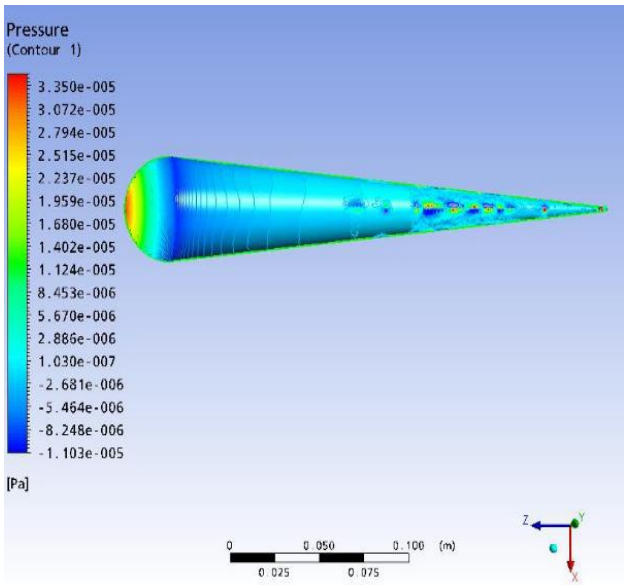

Figure 10. Pressure distribution for 250 mm tail length (0.0058m/s)

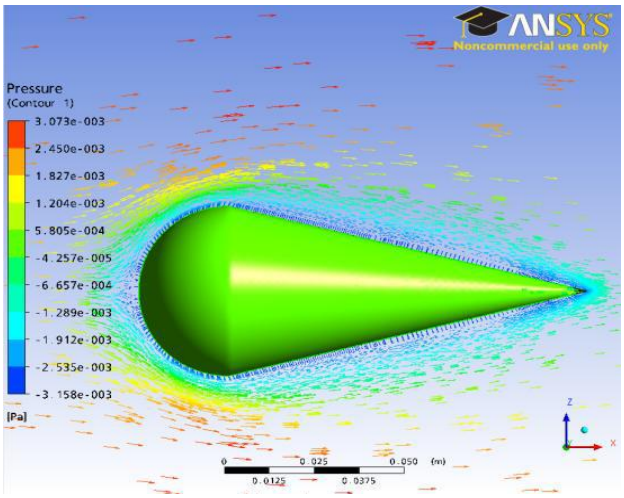

Figure 11. Pressure distribution for 200 mm tail length(0.0058 m/s)

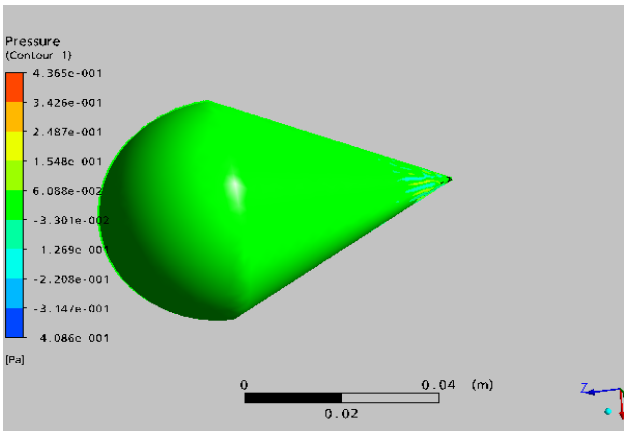

Figure 12. Pressure distributions for 50 mm tail length(0.0058m/s)

According to the figures (11, 12) at low velocity cases (0.0058 m/s), the pressure is vary insignificantly because the flow is smooth and the occurrence of turbulence is minimal apart comparing to the figure-10, which is the longest tail. As well as, the effect of long tail is also seen here. For the long tail case (figure 10 above), there were few instances (especially at the tail end) where pressures rises a little higher than the average. However, for the shorter tail case (figure 11 and 12) are not occur (the pressure is almost extremely uniform). Moreover, the pressure distribution at the intermediate mean flow velocity of 116.83 m/s shows a pattern that is intermediate between the patterns at 233.67 m /s and 0.0058 m /s respectively for the different cases.

C. CFD Derived Results

In order to calculate a poly line is placed around the model and the pressure on the nodes of the poly line exported into an excel file. Through this method, it can be demonstrated to check the y+ values around the body to confirm the quality of the mesh. The pressure over the body was used to calculate the drag and therefore the drag co-efficient for each of the 3 teardrop shapes. This was done by integrating the pressure difference over the area of each teardrop, see Equation 2. The mesh nodes were used as a distance between each calculation.

The pressures found on the turbulent models at velocity of (233 and 116 m/s) are very high. The laminar flow analysis gives very low drag calculation. Therefore, the calculated drag coefficient values are close to the expected drag co-efficient of 0.03-0.05 as explained in the figure-13 below. In theory, the drag co-efficient model should decrease with increasing tail length as it gets closer to the ideal L/D ratio of 4.5. Thus, it can be seen, the lowest drag co-efficient on A and B models.

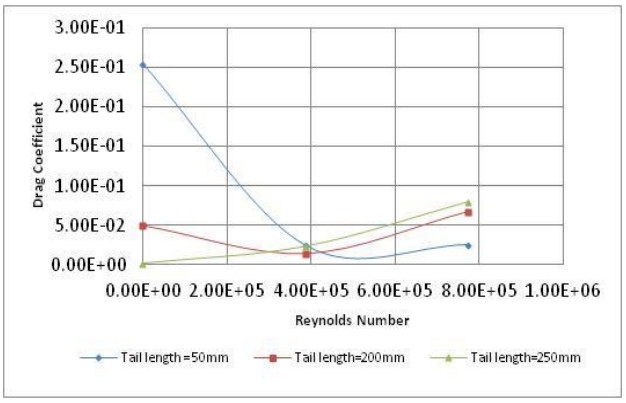

Figure13. Drag co-efficient v.s Reynolds number

IV. Conclusions

The geometry chosen was a large rectangular bounding box to give the space for the flow to develop. The size of the box was refunded using 2 dimensional analyses at high speed. This showed that the pressure increase at the edges of the box could not interfere with the flow around the teardrop. For this modeling study the pressure was on or very close to the body. Therefore, it can be prioritized for meshing strategy in this area and encountered difficulties in meshing the geometry; such difficulties were the point at the end of the tail. This was a balance between maintaining the teardrop shape and meshing the shape properly. There were limitations on the meshing strategy. The meshing strategy was universal for all models; therefore, there was scope to increase the total number of nodes for smaller models. Whereas, it can be confirmed that, the mesh was appropriate for the analyses, as convergence was reached to a low residual. For laminar flow the analyses never converged.

According to the comparing results from (k-epsilon) and the sheer stress transport turbulence models (SST), it therefore can be confirmed that the best model for this project was the SST. The main benefit from using SST, it was more able to model the boundary layer. The pressure results from k-epsilon analyses compared to the results from the SST analysis are markedly different. Therefore would have given very different drag co-efficient results. The validity of the model was confirmed by studying the pictorial representation of the pressure contours and velocity vectors. It could be seen that the smaller models had a more interesting flow features due to the gradient of the tail. On the other hand, the source of error between the predicted forces and the expected values comes from the integration process. Therefore, the simulation cannot capture the same level of variation that the body in a physical experiment, due to the limits of the computer simulation. This would be the case even if the values of the pressure at all the mesh points on the surface were exacted.

References

[1] Makino, Mitsuo. Hydrodynamic Drag and Stream-lined Form. s.l. : Sangyo-tosyo, 1991.
[2] Munson, Young, Okishi. Fundamentals of Fluid Mechanics .s.l. : Wiley, 2005 (5th Edition). ISBN: 978-0471675822 .
[3] Shaw, CT. Using Computational Fluid Dynamics. New York : Prentice Hall, 1992.
[4] The Element Of Aerofoil and Airscrew theory By H. Glauert
[5] Developing Wind PowerProjects : Theory and Practice By Tore Wizelius
[6] Flight Theory And Aerodynamics : A Practical guide for Operational safety By Charles E. Dole, James E. Lewis
[7]G.V.Parkinson and G.D.watt “Some new applications of linearized airfoil theory” (1983)
[8] Ghias, R., Mittal, R., and Lund, T., “A Non-Body Conformal Grid Method for Simulation of Compressible Flows with Complex Immersed Boundaries,” AIAA Paper 2004-0080, 2004
[9] Alex Sullivan Cleveland, F. A., “Aerodynamic forces acting on an airfoil”
[10] W. Kieffer, S. Moujaes, N. Armbya “CFD study of section characteristics of Formula Mazda race car wings” March 2005
[11] F. Muyl, Laurent Dumas, Vincent Herbert “Hybrid method for aerodynamic shape optimization”, June 2003.
[12] G.de Vahl Davis and C. Fletcher, “Computational Fluid Dynamics”. Amsterdam : Elsevier Science Publishers B.V., 1988, pp 315 – 328
[13] Hiroshi China, Masahiro Yoshida, Morihiro Takada, Kunio Nakagawa, “Air flow control around the cabin of a convertible car” July 1994
[14] AJ Scibor - Rylski, “Road Vehicle Aeerodynamics” London: Pentech Ressl, 1975, ch 1-7.
[15] R.W. Fox and A.T. McDonald, Introduction to Fluid Mechanics ~Wiley, New York, 1973!.
[16] M.E. Cates, J.P. Wittmer, J.-P. Bouchaud, and P. Claudin, Phys. Rev. Lett. 81, 1841 ~1998!; M.E. Cates and J.P. Wittmer, Physica A 263, 354 ~1999!.
[17] A.J. Liu and S.R. Nagel, Nature ~London! 396, 21 ~1998!.
[18] C. Liu et al., Science 269, 513 ~1995!; D.M. Mueth, H.M. Jaeger, and S.R. Nagel, Phys. Rev. E 57, 3164 ~1998!.
[19] B. Miller, C. O’Hern, and R.P. Behringer, Phys. Rev. Lett. 77, 3110 ~1996!.